



Contents lists available at ScienceDirect



Catalysis Today

journal homepage: www.elsevier.com/locate/cattod

Selective oxidation of ethanol to acetaldehyde over Au–Cu catalysts prepared by a redox method

Elena A. Redina ^{*}, Alexander A. Greish, Igor V. Mishin, Gennady I. Kapustin,
Olga P. Tkachenko, Olga A. Kirichenko, Leonid M. Kustov

N.D. Zelinsky Institute of Organic Chemistry, Russian Academy of Sciences, 47 Leninsky Prospect, Moscow 119991, Russia

ARTICLE INFO**Article history:**

Received 26 August 2013

Received in revised form 7 November 2013

Accepted 10 November 2013

Available online xxxx

Keywords:

Low-loaded gold-copper catalysts

Redox method

Selective ethanol oxidation

Acetaldehyde

ABSTRACT

A series of the Au–Cu/SiO₂ catalysts including low-loaded samples with an overall metal content less than 0.5 wt% was synthesized by a redox method. The catalysts were tested in the selective oxidation of ethanol to acetaldehyde. The highest catalytic activity was observed for the catalysts having the lowest metal content due to the presence of nanosized Au particles and the synergistic effect of Au–Cu²⁺ interaction. Unusual reduction behavior was found for the catalysts with the 0.2 wt% content of Cu. XRD, TPR, EXAFS, and STEM techniques were applied for the catalysts characterization.

© 2014 Elsevier B.V. All rights reserved.

1. Introduction

Selective oxidation of ethanol to acetaldehyde by oxygen over heterogeneous catalysts is of great interest as this process can replace the conventional one based on the oxidation of ethanol with very hazardous agents, such as chromate or permanganate [1]. Some essential results were obtained in the oxidative conversion of ethanol over noble metal-based catalysts, but fast deactivation of the catalysts and their overoxidation were observed [2]. Also, acetaldehyde was selectively produced by dehydrogenation of ethanol on the Cu containing catalysts [3] and by selective oxidation of ethanol over such catalysts as V₂O₅/TiO₂–SiO₂ [4], FeSBA-15 [5], supported manganese oxide [6] and graphite nanofibers [7]. However, in these cases, the catalysts revealed either a good selectivity in the limited range of the ethanol conversions (not exceeding 50%) or a low selectivity to acetaldehyde.

Supported gold catalysts can exhibit both high activity and selectivity in the oxidation of various alcohols, such as polyols [8,9], aliphatic [10,11], aromatic alcohols [12,13].

Rossi and Biella [14] studied the gas phase oxidation of primary and secondary alcohols over the 1% Au/SiO₂ catalyst, and in this case the selectivity to corresponding aldehydes and ketones reached around 100%. This catalyst was also active in the liquid phase ethanol oxidation to acetic acid [15] as well as the Au/MgAl₂O₄

catalyst [16]. The Au/CeO₂ catalyst [17], Au supported on hydroxylate [18,19] and Au supported on other metal oxides [20,21] were applied for the conversion of ethanol to carbonyl compounds. A high selectivity to acetaldehyde was also obtained in ethanol oxidation over the 1% Au/MoO₃ catalyst [1] and Au/TiO₂ with an Au content 0.5–7 wt% [22,23].

Of particular interest are the catalysts on the basis of the Au–Cu composition. For instance, the Au–Cu/SiO₂ catalyst appeared to be active in the benzyl alcohol oxidation to benzaldehyde providing the 98% yield, the oxidation efficiency of the bimetallic catalysts exceeded that of the monometallic systems, such as Au/SiO₂ and Cu/SiO₂ [13]. But, there are only a few works concerning ethanol oxidation over Au–Cu catalysts, in spite of the wide use of individually supported gold and copper in this reaction. A synergistic effect of Au and CuO_x constituents was revealed in the Au–Cu/SiO₂ catalyst which had a core-shell structure and was capable of catalyzing partial oxidation of ethanol to acetaldehyde. In the authors' opinion [24], both the high oxidation activity and selectivity of this catalytic system are caused by a close contact between the Au core and the CuO_x shell.

The present work is devoted to selective oxidation of ethanol to acetaldehyde with air over the Au–Cu catalysts prepared by a redox method. An intimate contact between two metal constituents in the catalyst structure was provided by selective Au deposition on the surface of Cu nanoparticles through the surface redox reactions between the oxidized form of Au and metallic Cu [25,26]. Main attention was paid to the preparation of the Au–Cu catalysts with the total metal loading not exceeding 0.5 wt%

* Corresponding author. Tel.: +7 9152694149.

E-mail address: redinalena@yandex.ru (E.A. Redina).

2. Experimental

2.1. Catalyst preparation

A commercial SiO₂ (Russia) was used as a support for the catalysts. Silica was chosen as a support to avoid undesirable side reactions initiated by the carrier itself. Physical characterization of the carrier was made using ASAP 2020 (Micromeritics). The surface characteristics were as follows: the BET surface area was 218 m²/g; the BJH pore volume was 0.81 cm³/g. The pore size distribution was rather narrow; the average value was 13.3 nm. The fraction of micropores did not exceed 1% of the total pore volume.

Metal precursors and other chemical reagents were of the analytical grade: Cu(NO₃)₂·3H₂O (Acros Organics) and HAuCl₄·3H₂O (Aurat), NaBH₄ (Sigma Aldrich).

2.1.1. Preparation of the Au/Cu/SiO₂ catalyst by the redox reaction (RR)

Preparation of the supported Au–Cu catalysts involved two stages:

- (i) Synthesis of the monometallic parent CuO/SiO₂ catalyst was performed by the incipient wetness impregnation of the support with an aqueous solution of Cu(NO₃)₂·3H₂O ($C=0.174\text{ M}$) for 1 h followed by drying at RT and at 60 °C overnight, then calcination at 400 °C for 4 h was performed. The wet impregnation was used for the preparation of high-loaded samples. In this case, a sample was dried under the vacuum using the rotary evaporator at 80 °C until obtaining the dry residue and then it was calcined at 400 °C for 4 h. The calcination temperature was chosen on the basis of the TG-DTA data.
- (ii) To obtain metallic copper supported on SiO₂ the reduction of the CuO/SiO₂ catalyst was carried out in the hydrogen flow (30 ml/min) at 400 °C for 2 h. At the end of this procedure the reactor was cooled to RT and the required amount of the HAuCl₄·3H₂O solution ($7.68 \times 10^{-3}\text{ M}$) was added to the solid, while the contact with atmosphere was excluded. The suspension obtained was left overnight. Then a solution was separated from the solid and the latter was washed several times with the deionized water to remove adsorbed Cl[−] ions and molecular Cl₂ from the catalyst surface. The amount of gold left in the solution was measured by the reverse iodometric titration. In all cases, the gold deposition on the catalyst surface was close to 99%. Finally, the sample was dried at 60 °C overnight.

The Au–Cu catalyst samples prepared by the redox method differed by either the Au/Cu atomic ratios (0:1; 1:3; 1:8; 1:0) or the weight percentage of the metals at the constant atomic ratio (0.2–5 wt% for each metal). The metal loadings were calculated using the following equations:

$$\omega(\text{Cu}) = m(\text{Cu}) 100\% / m(\text{support})$$

$$\omega(\text{Au}) = m(\text{Au}) 100\% / m(\text{support}) + m(\text{Cu})$$

The catalysts were marked as $x\%$ Au/ $y\%$ Cu/SiO₂ for the bimetallic catalysts and $y\%$ Cu/SiO₂ for the monometallic CuO/SiO₂ sample, where $x\%$ was the weight percentage of deposited Au and $y\%$ was the weight percentage of deposited Cu.

2.1.2. Preparation of the Au/SiO₂ and Au/Cu/SiO₂ catalysts by incipient wetness impregnation followed by NaBH₄ reduction

This method was described in [27]. SiO₂ was impregnated with an aqueous solution of HAuCl₄·3H₂O under stirring by a glass rod. For the bimetallic Au–Cu catalyst, the co-precipitation with the use of HAuCl₄·3H₂O and CuCl₂·3H₂O was applied. A solution of NH₄OH

(1.1 M) was added after 30 min a to the solid ($n_{\text{Au}}:n_{\text{NH}_4\text{OH}} = 1:55$) and the suspension was stirred for 10 min followed by addition of NaBH₄ ($n_{\text{Au}}:n_{\text{NaBH}_4} = 1:6.26$). Then the suspension was heated up to 60 °C and stirred for 10 min. The solid product was separated from the parent solution by centrifugation and washed several times with distilled water to remove Cl[−] ions from the catalyst surface. During the procedure, the partial reduction of gold in the solution took place. The Au and Au–Cu catalysts prepared by this method were marked as $x\%$ Au/SiO₂ and $x\%$ Au/ $y\%$ SiO₂–NaBH₄. The 0.8% Au/2% Cu/SiO₂–NaBH₄ catalyst was prepared as a reference to compare the activities with the catalyst having the same metal content, but prepared by a redox method.

2.2. Catalyst testing

The reaction was carried out in the glass reactor ($d_{\text{in}} = 5\text{ mm}$) with a fixed catalyst bed. The reactor was equipped with a temperature controller; the end of the thermocouple was placed near the bottom of the catalyst bed. The reaction was performed in the 50–450 °C temperature range at an atmospheric pressure. Before the run, the catalyst (~0.1 g) was treated at 300 °C for 1 h in an air–He flow. The feed gas consisted of 1% C₂H₅OH (96%, Bryncalov Ferein), 1.2% O₂ (from air) and He. Ethanol was supplied by the micropump. Ethanol was mixed at the inlet of the reactor with the gas flow. The gas flow rate of 21 ml/min was maintained by a flow controller, VGSH was 4800 h^{−1}. The blank test confirmed that in the absence of the catalyst no reaction occurred.

The analysis of the reaction products was performed by a gas-liquid chromatograph equipped with a TCD detector. The oxygen-containing compounds such as ethanol, acetaldehyde, diethyl ether, and ethyl acetate were analyzed by the Chromatec – Crystall 5000.2 chromatograph with the Carbowax 6000 stainless steel column (3 mm × 2.5 m). The gaseous products such as H₂, CO, CO₂ and ethylene were analyzed by the LKhM-8D chromatograph equipped with a stainless steel column (3 mm × 6 m) packed with Porapak Q.

The carbon balance in all catalytic experiments was no less than 99%.

2.3. Catalyst characterization

2.3.1. XRD

The phase composition of the catalysts and the particle size of the supported metal were examined by X-ray diffraction (XRD) analysis. X-ray diffraction patterns were recorded using a DRON-2 diffractometer with Ni-filtered Cu K α radiation ($\lambda = 0.1542\text{ nm}$) in a step scanning mode, with a step of 0.02° and a counting time of 0.6 s per step in the range of $2\theta = 20^\circ$ –80°. Identification of the phases was performed by comparison of the position and intensity of the peaks with the data from the files of International Center for Diffraction Data. The crystal size of nanoparticles was calculated from X-ray peak broadening.

2.3.2. TPR-H₂

TPR measurements were performed in the lab-constructed flow system. The Cu/SiO₂ catalyst sample with a weight of 150 mg was pretreated in an argon flow at 150 °C for 60 min. For the gold containing catalysts, the pretreatment was carried out at 80 °C for 120 min. Then the catalyst sample was cooled in the Ar flow to –50 °C prior to the TPR experiment. The heating from –50 to 850 °C was carried out at the rate of 10 °C/min in the 4.6% H₂ – Ar gas mixture supplied with a space velocity of 30 ml/min. Then the sample was kept at 850 °C until the hydrogen consumption ceased.

2.3.3. STEM

The powder samples were placed on the fixed copper netting with $d=3$ mm. The microstructure of the samples was studied by means of scanning transmission electron microscopy with a field emission (FE-STEM) Hitachi SU8000 microscope. The experiment was performed in the light field mode by registering transmitted electrons under the accelerating voltage of 30 kV.

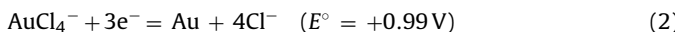
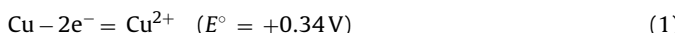
2.3.4. XAS

XAS (XANES + EXAFS) measurements were carried out in HASY-LAB (DESY in Hamburg, Germany) on the beamline C1 (Au L₃-edge, 11,919 eV, and Cu K-edge, 8979 eV) using a double-crystal Si(311) monochromator, which was detuned to 50% of the maximum intensity to exclude higher harmonics in the X-ray beam. The spectra were recorded in the transmission mode at a low temperature ($T=80$ K) in order to decrease the Debye–Waller factors. All spectra were measured simultaneously with the reference spectrum of Au or Cu foil placed behind the second ionization chamber, so that the absolute energy calibration was performed.

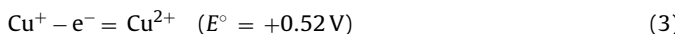
3. Results and discussion

3.1. Catalyst preparation by the redox method

A series of silica-supported Au–Cu catalysts was synthesized by the redox method using HAuCl₄ as the Au precursor. We varied both the Au/Cu atomic ratio (1:0, 1:3, 1:8, 0:1) and the content of each metal (0.2–5 wt%) while keeping the Au:Cu atomic ratio unchanged. The redox method applied for Au deposition is based on the surface redox reaction between metallic copper and oxidized gold via semi-reactions 1–2 shown below [25,28]:



As far as the standard redox potential of gold is higher than that of copper, the Au oxidized form can be readily reduced by Cu⁰, while Cu⁰ oxidizes to Cu²⁺ (CuO). The amount of Cu oxidized by Au³⁺ should be equal to the molar Au/Cu ratio. To study the reduction conditions and behavior of supported copper oxide, the method of temperature-programmed reduction with hydrogen was applied. The data revealed that the reduction temperatures depended on the copper content in the catalyst. A two-step reduction behavior of the copper oxide species with high-temperature peaks (above 600 °C) was observed (see below). The temperature of copper oxide reduction in the Cu containing samples was chosen as 400 °C in order to avoid sintering of Cu nanoparticles. The TPR-H₂ data allowed us to suppose that copper oxide species are not fully reduced to Cu⁰, and it is necessary to add the third possible semi-reaction, as follows:



3.2. Characterization of the catalysts by physico-chemical methods

3.2.1. XRD

The XRD patterns of the catalysts are given in Figs. 1–3. One can see that for all Au-containing samples the most intense line is observed at $2\theta=38.2^\circ$, and it can be attributed to the Au(111) plane.

For the monometallic 0.8% Au/SiO₂ catalyst (Fig. 1), one more peak appears at 44.4° , it is observed for both fresh and used samples. The X-ray line broadening analysis revealed the average gold particles size to be about 8–10 nm.

The XRD pattern of the 0.8% Au/0.8% Cu/SiO₂ sample (Fig. 2a) contains two lines at $2\theta=38.2^\circ$ and 44.4° corresponding to Au⁰.

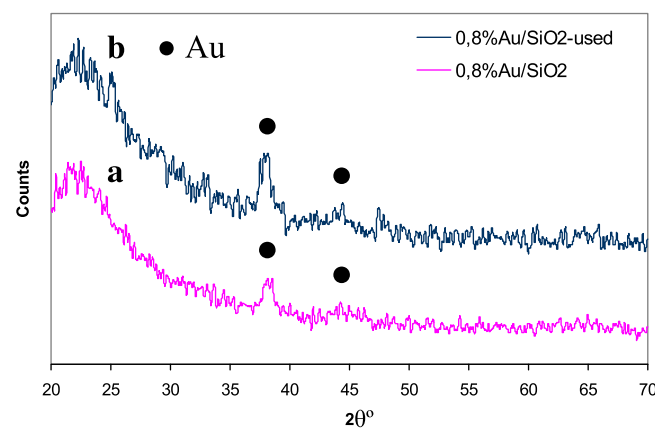


Fig. 1. XRD patterns of the 0.8% Au/SiO₂ catalyst: fresh (a); used (b).

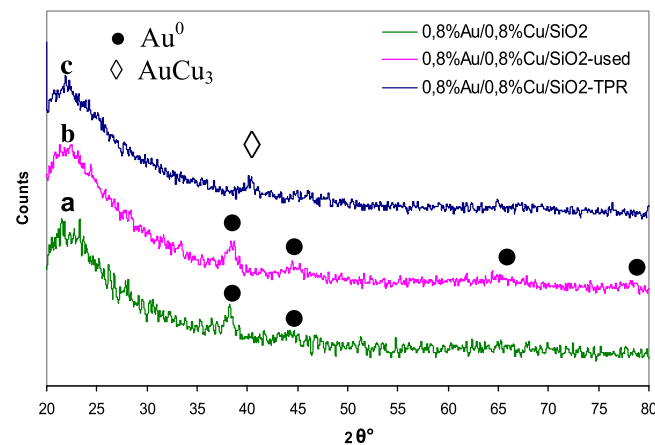


Fig. 2. XRD patterns of the 0.8% Au/0.8% Cu/SiO₂ catalyst: fresh (a); used (b); after reduction at 25–850 °C (c).

The average size of Au particles in the fresh sample was found to be 8 nm, after using the catalyst in the reaction for three times and more there was no increase in the Au crystalline size (Fig. 2b). Furthermore, the reduction of this sample at 25–850 °C led to the shift of the peak at $2\theta=38.2^\circ$ to the position at $2\theta=40.5^\circ$, which corresponds to the AuCu₃ alloy (Fig. 2c). The average size of the alloy crystallites was found to be also 8 nm.

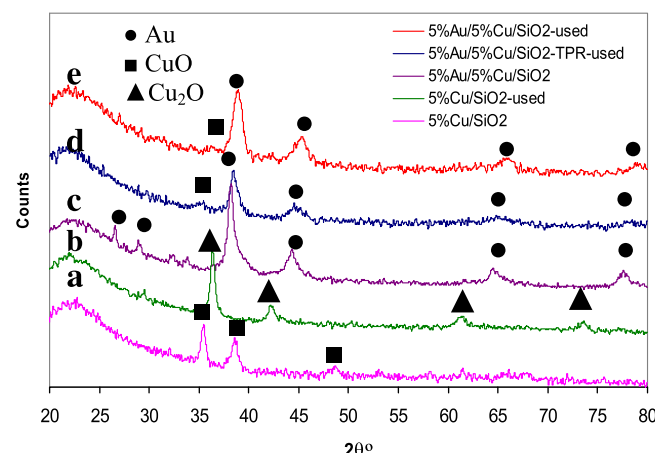


Fig. 3. XRD patterns of the 5% Cu/SiO₂ sample: fresh (a), used (b); and of the 5% Au/5% Cu/SiO₂ catalyst: fresh (c), used after reduction at 25–850 °C (d), used (e).

Table 1

TPR study results of the Au–Cu samples prepared by a redox method.

Catalyst	Au:Cu	CuO content (mol 10 ⁶)	H ₂ consumption (mol 10 ⁶)	H ₂ : CuO	T _{max} (°C)
0.2% Cu	–	5.44	26.2	4.82	380, 609 (shoulder), 639, 662
0.2% Au/0.2% Cu	0.32	9.46	10.6	1.12	268, 350, 510, 664
0.8% Cu	–	18.9	9.52	0.50	260, 674
0.8% Au/0.8% Cu	0.32	18.7	47.8	2.56	280, 550, 677
5% Cu	–	80.1	85.3	1.06	248, 295, 644
5% Au/5% Cu	0.32	80.7	24.1	0.30	239, 259, 302 (shoulder)

The XRD patterns obtained for the fresh and used 5% Cu/SiO₂ catalysts are given in Fig. 3. The intense peaks at 2θ = 35.5° and 38.7° for the fresh sample (Fig. 3a) were ascribed to the (111) plane of CuO. The XRD analysis of the used 5% Cu/SiO₂ catalyst revealed only the existence of the Cu₂O phase, with an average particle size of 18 nm (Fig. 3b). During the reaction, a partial reduction of Cu²⁺ to Cu⁺ is possible due to the coke formation. Such conversion of the Cu species was estimated in [24] by the XPS method.

The XRD spectra of the fresh 5% Au/5% Cu/SiO₂ sample reveal resolved sharp peaks of Au⁰, but surprisingly, there were no signals of CuO phase (Fig. 3c). Such phenomenon was also observed in [23]. An average size of the Au particles was found to be in the range of 9–10 nm. Employment of the catalyst in the oxidation reaction led to some changes in the catalyst structure. The XRD pattern of the 5% Au/5% Cu/SiO₂ catalyst used in ethanol oxidation exhibits the peaks assigned to Au⁰ and the CuO phase. The peaks attributed to Au and CuO shifted by 0.5° to the higher values of 2θ, which pointed to the alloy formation during ethanol oxidation. This effect was not found for this sample which was preliminarily reduced before the catalytic experiment.

The peaks of the CuO phases were not detected in the XRD patterns for the catalyst samples in which the Cu content was less than 2 wt%, even after catalytic runs or high temperature treatment under the TPR-H₂ conditions. The reason was either a small size

of the crystallites (less than a detection limit) or low contents of the mentioned phases in the samples. No signals assignable to Au⁰ were detected in the low-loaded samples; this could be caused by the same reasons.

3.2.2. STEM

STEM images of the 0.8% Au/0.8% Cu/SiO₂ sample show that metal nanoparticles (NPs) are uniformly dispersed on the support surface (Fig. 4). The wide distribution of metal particles was observed for both fresh and used samples. The catalytic reaction caused changes in the distribution of the Au particle size. After the reaction, a part of the metallic NPs fractions with d = 5–7 nm and d = 13–15 nm decreased, while a part of the NP fraction with d = 9–11 nm increased in about 1.5 times. At the same time, the formation of agglomerates with d > 20 nm was observed too. Anyway, after the reaction the average particle size did not change significantly and the most abundant metal NPs size was in the range of 7–9 nm for both the fresh and used samples that was in a good agreement with XRD data.

3.2.3. TPR-H₂ study

It was found that the reduction behavior of the catalyst samples in the TPR-H₂ study depended on the amount of Cu loaded in the catalyst. The latter affected the reduction degree of the bimetallic

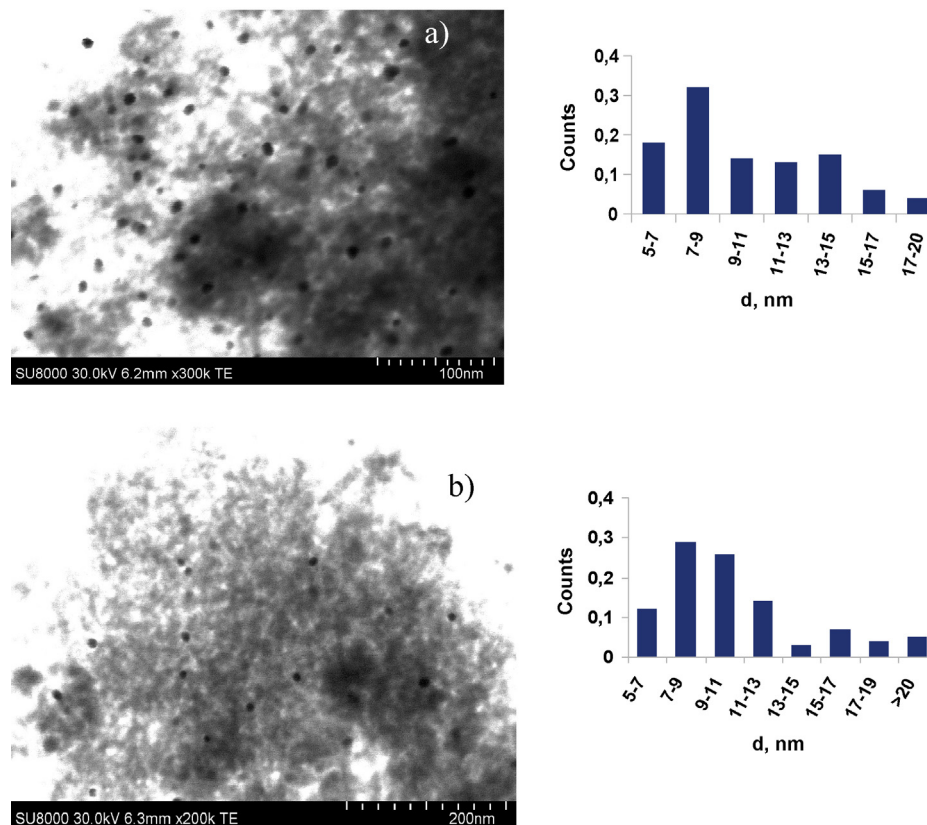


Fig. 4. STEM images and particle size distribution for the 0.8% Au/0.8% Cu/SiO₂ catalyst: fresh (a), used (b).

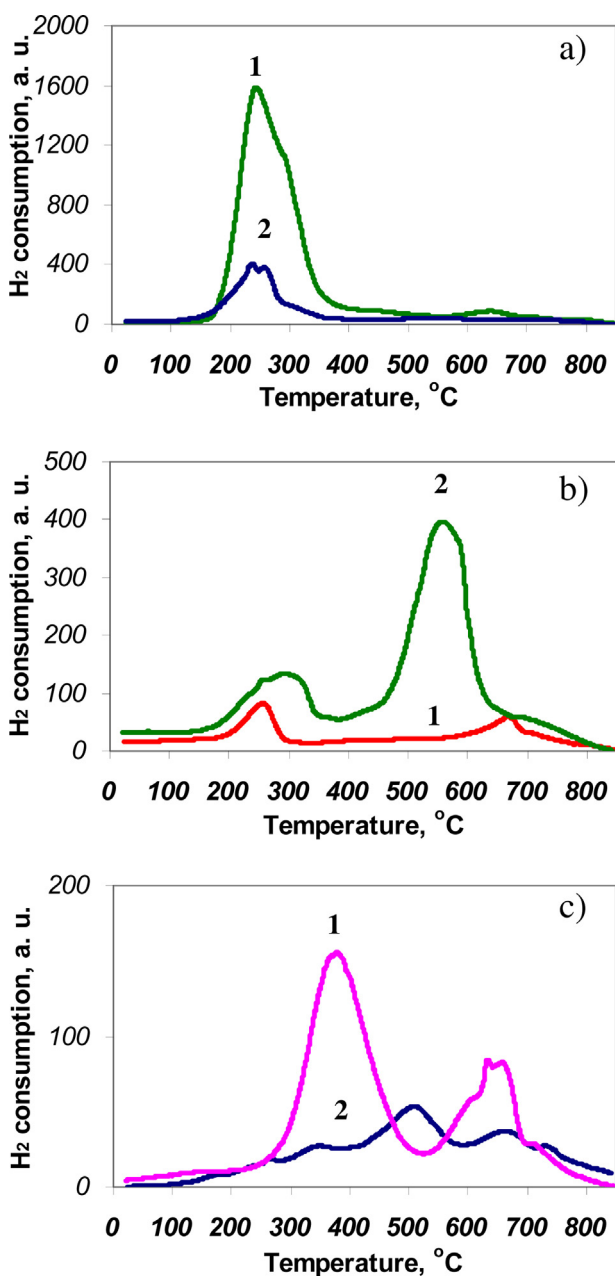


Fig. 5. TPR profiles of the catalysts: (a) 5% Cu/SiO₂ (1), 5% Au/5% Cu/SiO₂ (2); (b) 0.8% Cu/SiO₂ (1), 0.8% Au/0.8% Cu/SiO₂ (2); (c) 0.2% Cu/SiO₂ (1), 0.2% Au/0.2% Cu/SiO₂ (2).

Au–Cu catalyst after Au deposition. The TPR-H₂ results are presented in Fig. 5.

The TPR-H₂ profile of the 5% Cu/SiO₂ sample (Fig. 5a) manifests two intensive peaks: the main peak with a maximum at 250 °C and a shoulder at 295 °C and a small peak with a maximum at 640 °C. These peaks were ascribed to the reduction of the CuO nanoparticles (250 °C) and to the stepwise reduction of Cu²⁺ ions to Cu⁺ (295 °C) and Cu⁺ to Cu⁰ (640 °C) [29]. The amount of the hydrogen consumption coincides with the amount of copper oxide supported, thereby indicating the complete reduction of CuO.

After deposition of 5 wt% Au on the surface of Cu⁰ particles in 5% Cu/SiO₂ sample by the redox reaction, the hydrogen consumption was observed also, although its value was smaller than for 5% Cu/SiO₂ (Table 1). Following the redox method, reduced copper was oxidized to Cu²⁺ by Au³⁺ in the surface redox reaction. According to the results, the molar H₂: Cu ratio is 0.3, that is almost equal to the

molar Au:Cu ratio, 0.32. This fact can be considered as an evidence of the metallic Au deposition directly on the Cu species when using the redox method. During the TPR procedure, CuO was reduced (Fig. 5a), thus resulting in the double peak at lower temperatures, at 240 °C and 263 °C, the appearance of which can be explained by the same reduction processes described above for the 5% Cu/SiO₂ catalyst and different Cu-NPs size. The existence of the peak shoulder at 310 °C and the disappearance of the peak at 640 °C obtained while 5% Cu/SiO₂ sample reduction point to more facile reduction of Cu⁺ species before their interaction with SiO₂ because of direct Au–CuO_x contact takes place.

Quite a different reduction behavior was observed for the samples characterized by a lower Cu content. The TPR profile of the 0.8% Cu/SiO₂ sample (Fig. 5b) shows the two-step reduction. The first peak at 260 °C can be ascribed to the reduction of CuO_x clusters to Cu⁰ and the partial reduction of the isolated Cu²⁺ species to Cu⁺. The second peak at a significantly higher temperature, 674 °C, probably corresponds to the reduction of isolated Cu⁺ to Cu⁰ [30]. The reduction of the supported copper oxide with 0.8 wt% Cu was not complete and only 50% of the CuO phase was reducible (Table 1). This could be accounted for by the presence of the isolated Cu²⁺ ions, which were more difficult to be reduced in comparison with the small CuO_x particles because of the stronger interaction with the support [31]. As compared to the sample with a higher copper content, the reduction profile peak of the 0.8% Cu/SiO₂ sample was slightly shifted to the higher temperatures due to the stronger interaction between the Cu²⁺ ions and the support.

Two peaks were characteristic of the TPR curves of the 0.8% Au/0.8% Cu/SiO₂ sample (Fig. 5b). Deposition of gold (at the Au:Cu = 1:3 atomic ratio) on the Cu/SiO₂ catalyst led to unusual excess of hydrogen consumption during the TPR run. The first peak of hydrogen consumption was observed at 280 °C and related with the reduction of the small CuO_x clusters and the large CuO particles, which occurred in the sample, according to the STEM data. The second high-temperature reduction peak was detected at 564 °C. This can be ascribed to the peak observed for the 0.8% Cu/SiO₂ sample at 674 °C shifted to lower temperatures for the Au–Cu catalyst indicating the facilitated reduction of copper oxide species. It was found that the molar quantity of hydrogen consumed was twice higher than the molar amount of the supported copper oxide.

Almost a fivefold excess in hydrogen consumption was detected in the TPR study of 0.2% Cu/SiO₂ (Table 1). Two types of the reduction peaks were also observed (Fig. 5c). The first peak (at 380 °C) was caused by the reduction of isolated Cu²⁺ ions interacting with the SiO₂ support. As compared with the 0.8% Cu/SiO₂ sample, the first reduction peak was obtained at higher temperatures due to stronger interaction between Cu²⁺ and SiO₂. The complicated reduction behavior was observed at temperatures above 600 °C. Three peaks, at 609, 639, and 662 °C, were overlapped. These peaks can be attributed to the reduction of isolated Cu⁺ ions to Cu⁰ as it was mentioned above and/or to the reduction processes related to the support itself.

While comparing the 0.8% Au/0.8% Cu/SiO₂ sample with 0.2% Au/0.2% Cu/SiO₂, in the latter case the Au deposition suppressed the processes responsible for the additional hydrogen consumption. The maxima of the peaks were shifted to lower temperatures as a result of the easier reduction of the Cu²⁺ ions (Fig. 5c and Table 1). Anyway, the total reduction behavior of the 0.2% Au/0.2% Cu/SiO₂ sample was rather complex and it was difficult to assign all of the observed peaks to the processes that could proceed on the catalyst surface.

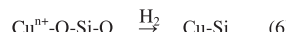
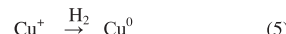
Noteworthy, these phenomena of the unusually high hydrogen uptake by the copper-containing supported systems (with low loadings) have not been mentioned elsewhere, to the best of our knowledge. The possible reactions are shown in Scheme 1. One of the reasons of the effects observed in this study can be the

First reduction peak:



Reduction peaks at the temperature above

600°C:



Scheme 1. Possible processes during reduction of CuO/SiO₂ and Au-Cu/SiO₂ catalysts in TPR-H₂ study.

hydrogen spillover described for such systems in [32]. For the bimetallic samples, the sequence of the reduction steps can be as follows: the dissociative hydrogen adsorption or the hydrogen spillover occurred on the surface of Au NPs with consequent reduction of the copper oxide species. Activated hydrogen adsorption also can take place on the periphery of the Au-Cu contact site, whereas the hydrogen spillover from Cu⁰ to silica is possible too. Dissociative adsorption of hydrogen on the Au-Cu alloy nanoparticles and the reduction of the support surface by the hydrogen spillover were observed for the Au-Cu/TiO₂ catalyst in [33]. In spite of that, the hydrogen spillover effect is considered to be common for “d-metal-reducible oxide” systems but not for the “metal-inert support” such as silica; however, this effect was proved for the Pt/Al₂O₃, Pt/SiO₂ [34]. Copper is known to be active for the hydrogen spillover as well. Thus, as it was described above, after the reduction of 0.8% Au/0.8% Cu/SiO₂ the AuCu₃ alloy formation was observed. This indicated strong interaction between Au-Cu-SiO₂ in the reduced sample and could lead to hydrogen spillover and SiO₂ reduction. Probably, in the 0.2% Au/0.2% Cu/SiO₂ catalyst the Cu²⁺-SiO₂ interaction was much stronger than Au-Cu, but it was weaker than in the 0.2% Cu/SiO₂ sample and hydrogen consumption was detected to be approximately equal to 1.

Silicide formation is to be considered after reduction of the 0.2% Cu/SiO₂ sample [35]. In addition, very strong interaction of Cu²⁺ with the support may lead to the reduction of silica and Cu²⁺ at the same time. Au deposition could make this interaction weaker.

3.2.4. EXAFS

3.2.4.1. Au L₃-edge. The Fourier transformation of the EXAFS oscillations of the Au sample and a reference are presented in Fig. 6. In the spectrum of the Au foil, the first double peak corresponds to

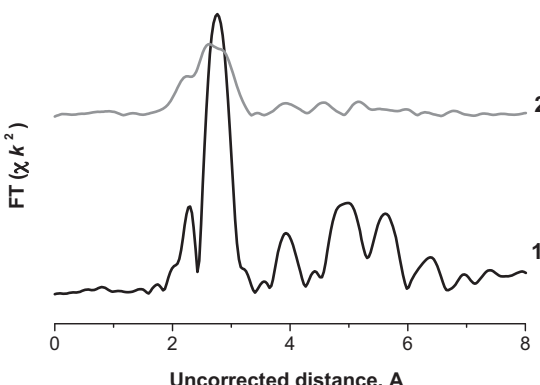


Fig. 6. FT Au L₃ EXAFS spectra of Au foil (1) and 0.8% Au/0.8% Cu/SiO₂ sample (2).

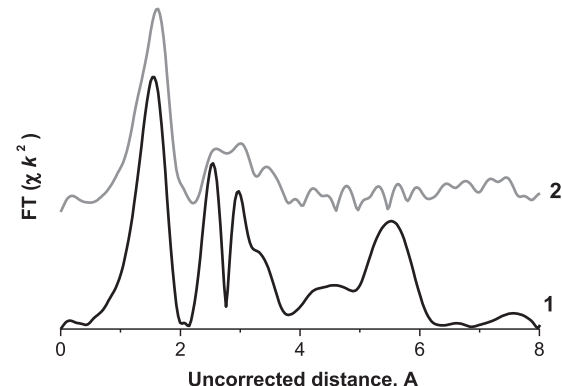


Fig. 7. FT Cu K EXAFS spectra of CuO (1) and 0.8% Au/0.8% Cu/SiO₂ sample (2).

the first coordination shell containing 12 Au atoms at a 2.885 Å real distance from the central Au atom.

The FT EXAFS oscillations of the Au-containing sample resembles the spectrum of the Au foil showing the metallic state of gold in this sample and differs from those of the Au foil in the intensity of the peaks. The Au spectrum of the sample may be readily fitted in both *r*- and *k*-spaces with a single-shell model – the gold shell around the central absorbing gold atom. The results of model fits of the EXAFS spectra are given in Table 2.

The analysis of the EXAFS oscillations shows that the nearest neighbors of the central Au atom in the samples are the Au atoms with an average coordination number (CN) about 10.8 at 2.85 Å real distances. With the assumption of a spherical shape, the average maximal sizes in the range of ~50 Å are obtained for the Au metal nanoparticles in this sample. Noteworthy, the presence of the long-distance peaks in the EXAFS spectra of the sample under study points out that the sample contains not only particles with the diameter 50 Å but also larger particles.

3.2.4.2. Cu K-edge. The Fourier transformation of the EXAFS oscillations of the Cu-containing sample and the reference are presented in Fig. 7. The spectrum of the sample resembles the spectrum of CuO, therefore the Cu²⁺ state predominates in these samples. In the spectrum of CuO, the first peak corresponds to two first coordination shells containing four Cu atoms at 1.951–1.961 Å real distances from the central Cu atom.

The FT EXAFS oscillations of the Cu-containing sample are close to that of the CuO reference in terms of the intensity and the position of the first peaks. The Cu spectrum of samples may be readily fitted in both *r*- and *k*-spaces with a single-shell model such as an oxygen shell around the central absorbing Cu atom. The results of model fits of the EXAFS spectra are collected in Table 2.

The analysis of the EXAFS oscillations shows that the nearest neighbors of the central Cu atom in the samples consist of O atoms with an average CN of 3.4–3.5 at 1.96–1.98 Å real distances. Noteworthy, the EXAFS spectrum of the Cu sample differs from that of CuO and this shows that copper species do not form an oxide phase. Probably they are bound with the support via oxygen of silanol groups of silica.

3.2.5. Catalysts testing in ethanol oxidation

The main product of ethanol oxidation over the prepared catalysts was acetaldehyde (AA) and CO₂ was obtained as the only by-product. When the reaction was performed at temperatures higher than 300 °C this led to complete EtOH oxidation to CO₂ and H₂O. The maximum AA yields were observed in the temperature range of 220–250 °C and the CO₂ selectivity varied from 0% to 30% depending on the catalysts composition. For all the gold-containing

Table 2

EXAFS data for the Au–Cu sample.

Catalyst	Path	r (Å)	CN	$\sigma^2 \times 10^{-3}$ (Å ²)	ΔE (eV)	D_{Au} (Å)
0.8% Au/0.8% Cu	Au-Au	2.85 ± 0.01	10.8 ± 0.2	8 ± 1	6 ± 1	42.6 ± 8.8
	Cu-O	1.97 ± 0.01	3.4 ± 0.1	6 ± 1	15 ± 1	—

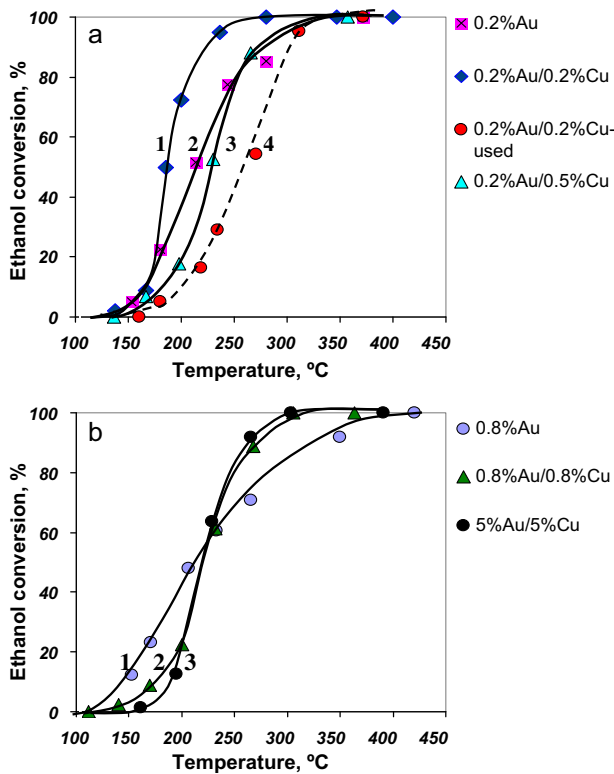


Fig. 8. a. Temperature dependence of the ethanol conversion over the catalysts: 0.2% Au/0.2% Cu/SiO₂ (1); 0.2% Au/SiO₂ (2); 0.2% Au/0.5% Cu/SiO₂ (3); 0.2% Au/0.2% Cu/SiO₂ – used (4). (b) Temperature dependence of the ethanol conversion over the catalysts: 0.8% Au/SiO₂ (1); 0.8% Au/0.8% Cu/SiO₂ (2); 5% Au/5% Cu/SiO₂ (3).

catalysts, the 50% conversion was reached if the reaction temperature was below 225 °C (Fig. 8a and b), 100% selectivity to AA having been observed. The lowest temperature for the 50% conversion was characteristic of the 0.2% Au/0.2% Cu/SiO₂ sample, namely 188 °C (Fig. 8a). Noteworthy, no products were detected when the reaction was carried out over the Au/SiO₂ catalyst at temperatures below 250 °C under the oxygen-free conditions. This proved that the reaction proceeded through the oxygen-assisted dehydrogenation of EtOH discussed in detail in [36–38].

In order to compare the efficiency of the prepared catalysts in the ethanol oxidation, a specific catalytic activity (SCA) was calculated as a quantity of AA (mol) produced per hour over the unit weight of Au (g) in each catalyst sample (Fig. 9).

According to our data, the higher was the gold concentration in the catalyst; the lower was the SCA of the gold nanoparticles in the Au monometallic catalysts. This was caused by an increase of the Au particle size detected by the XRD analysis. In the case of the monometallic Cu catalysts, a higher Cu concentration led to the higher values of the EtOH conversion but to the lower selectivity because of the intensification of complete oxidation of EtOH with formation of CO₂. As for bimetallic Au–Cu catalysts, the higher was the metal loading at the same Au:Cu atomic ratio the lower were SCA values (Fig. 9 and Table 3). At the same time, an increase in the copper content in the bimetallic catalysts at the same Au loading (Au:Cu = 1:8) resulted in the drop of the EtOH conversion, the selectivity to AA, and SCA as well (Figs. 9 and 10).

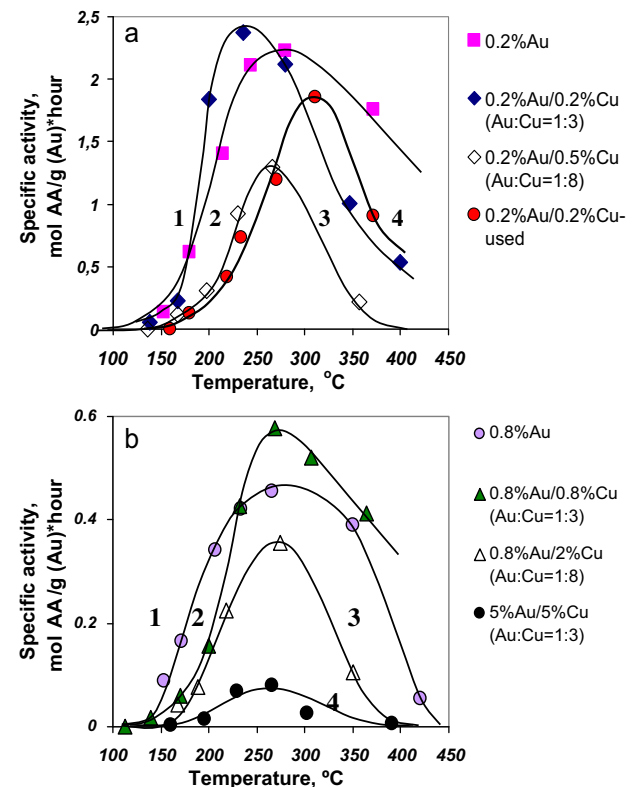


Fig. 9. (a) Temperature dependence of the specific activity for the catalysts: 0.2% Au/0.2% Cu/SiO₂ (1); 0.2% Au/SiO₂ (2); 0.2% Au/0.5% Cu/SiO₂ (3); 0.2% Au/0.2% Cu/SiO₂ – used (4). (b) Temperature dependence of the specific activity of the catalysts: 0.8% Au/0.8% Cu/SiO₂ (1); 0.8% Au/SiO₂ (2); 0.8% Au/0.2% Cu/SiO₂ (3); 5% Au/5% Cu/SiO₂ (4).

It follows from the data presented in Figs. 9 and 10 that the catalysts characterized by the atomic ratio Au:Cu = 1:3 manifest the higher values of the alcohol conversion and selectivity to AA in comparison with the monometallic Au and Cu catalysts having the same metal loadings. This proved the synergetic effect

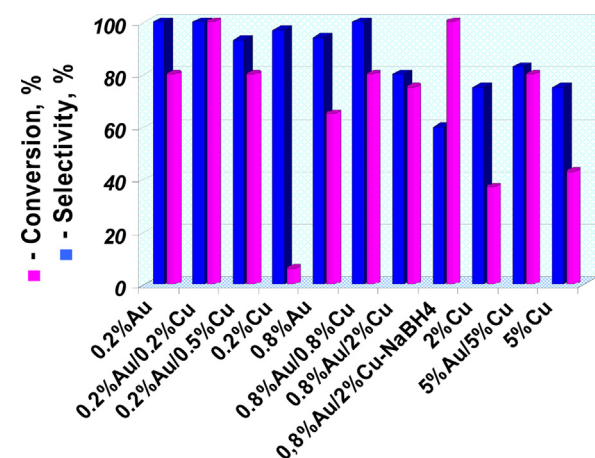


Fig. 10. Conversion and selectivity of the catalysts at 250 °C.

Table 3

Comparison of the catalysts.

Catalyst	$t = 250^\circ\text{C}$ Specific activity, mol (AA) g^{-1} Au (Cu) h^{-1}	d (Au/Cu), nm (XRD data)	Phase composition Au/Cu (XRD, TPR data)
0.2% Au	2.2	n.d.	n.d.
0.2% Au/0.2% Cu	2.4	n.d.	Au ⁰ /Cu ²⁺
0.2% Au/0.5% Cu	1.25	n.d.	n.d./CuO, Cu ²⁺
0.8% Au	0.43	8 (15) ^a	Au ⁰
0.8% Au/0.8% Cu	0.55	8 (3–5) ^b /n.d.	Au ⁰ /CuO, Cu ²⁺ ^b , Cu ⁰
0.8% Au/2% Cu	0.37	8/n.d.	Au ⁰ /CuO, Cu ⁰
0.8% Au/2% Cu-NaBH ₄	0.30	10/n.d.	Au ⁰ /CuO
5% Au/5% Cu	0.08	10/n.d.	Au ⁰ /CuO, Cu ²⁺ , Cu ⁰
0.2% Cu	0.3	n.d.	Cu ²⁺
2% Cu	0.06	11	CuO, Cu ²⁺
5% Cu	0.03	14 (18) ^a	CuO
0.2% Au/0.2% Cu-TPR	0.8	n.d.	n.d.
0.2% Au/0.2% Cu-used	1	n.d.	Au ⁰ /Cu ²⁺
0.8% Au/0.8% Cu-TPR	0.32	8	AuCu ₃
0.8% Au/0.8% Cu-used	0.42	8/n.d.	Au ⁰ /CuO, Cu ²⁺

^a After the catalytic test.^b According to the EXAFS data.

caused by Au⁰-Cuⁿ⁺ or Au⁰-CuO_x interactions. One can conclude from the values of SCA that if the reaction is performed in the 200–250 °C temperature range the highest activity was exhibited by the bimetallic catalyst with the lowest metal loading and the atomic ratio Au:Cu = 1:3, e.g. 0.2% Au/0.2% Cu/SiO₂. This catalyst provided the complete conversion of ethanol to AA with the 100% selectivity and a very high value of SCA.

The drop of the initial activity of the bimetallic Au-Cu catalysts with increasing metal loading at the constant Au:Cu atomic ratio was likely caused by the growth of both metal particles and transformation of the state of the copper species related with the increase in the copper loading, which was confirmed by XRD and STEM analysis. According to the XRD, TPR and EXAFS data, in the samples with Cu content in the range of 0.2–0.8 wt%, copper preferably existed in the form of the Cu²⁺ and Cu⁺ ions, while the CuO phase predominated in the samples having the higher copper loading. An increase in the atomic copper content led to the intensification of the complete oxidation of ethanol and thus to the lower values of the selectivity to AA and SCA. The obtained phase composition of the catalysts is presented in the Table 3.

If we compare the 0.8% Au/2% Cu/SiO₂ catalyst prepared by the redox method with the catalyst of the same composition but prepared by the NaBH₄-reduction technique, we can notice that the selectivity to AA and SCA for the latter catalyst is remarkably lower compared to the former catalyst (Fig. 10 and Table 3).

The most active sample, 0.2% Au/0.2% Cu/SiO₂, lost its activity after the run and the maximum value of SCA can be attained only at higher temperatures. However, the value of SCA obtained at 250 °C remained close to that of other Au-Cu samples or even higher, the catalyst keeping this SCA level during further three runs (Fig. 11). The decrease in the activity of the 0.2% Au/0.2% Cu/SiO₂ catalyst can be accounted for the sintering of the Au nanoparticles with a size of 3–5 nm, the existence of which was confirmed by EXAFS even for the sample with a higher Au content. STEM images of the 0.8% Au/0.8% Cu/SiO₂ sample indicated redistribution of the metal particle size after the catalytic reaction and a decrease of the amount of the fraction with an average size of 7 nm related with the formation of larger particles. Nevertheless, the most abundant particles were still those with the size about 8–10 nm. In addition, interdiffusion of Cu atoms in the SiO₂ outermost atomic layer and disappearance of the active sites located at the Au-CuO_x interface could lead to a drop in the catalytic activity of the low-loaded samples too [35].

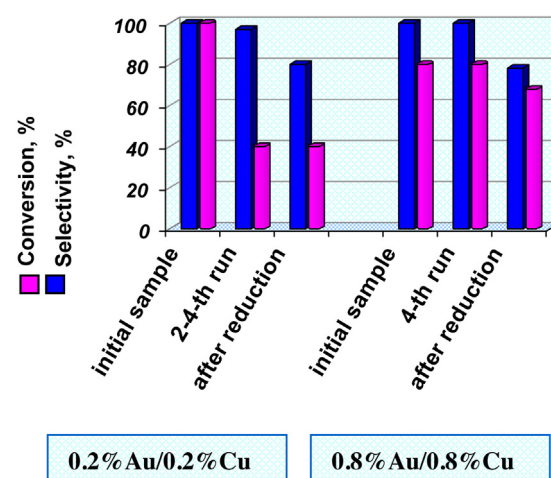


Fig. 11. Stability of the catalysts expressed in terms of the conversion and selectivity obtained at 250 °C.

The 0.8% Au/0.8% Cu/SiO₂ catalyst appeared to be the most stable system capable of maintaining its initial activity even after four runs (Fig. 11). Taking into account the data obtained, it can be concluded that metal nanoparticles with the average size of 8–10 nm were resistant against sintering under the reaction conditions and the particle growth proceeds until this value was reached.

Reduction in the hydrogen flow of the low-loaded samples at 25–850 °C led to a decrease in of the SCA, EtOH conversion and selectivity to AA (Fig. 11). The lower activity of 0.8% Au/0.8% Cu/SiO₂-TPR revealed after the high temperature reduction was due to the AuCu₃ alloy formation, which was proved by XRD analysis. An average Au and AuCu₃ crystalline size in fresh and reduced samples respectively was the same, about 8–10 nm. So, the differences in the activity of the fresh and reduced samples can be explained only by the different catalyst structure (Table 3). The higher activity of the silica-supported Au-CuO_x hybrid catalysts in the selective oxidation of ethanol into acetaldehyde in comparison with the silica-supported Au-Cu alloy nanoparticles was also observed in [24]. It should be noted that the same situation was observed for the Au-Ir/SiO₂ catalysts in gas phase ethanol oxidation to acetaldehyde when intimate contact between Au and IrO_x occurred [39].

4. Conclusions

The Au-Cu bimetallic catalysts with the different metal loadings were prepared by a very facile surface redox-reaction method. Defined synthesis of the catalysts by redox method allowed us to deposit Au NPs directly on the surface of copper oxide or Cu²⁺ species which was proved by TPR, EXAFS and STEM studies. The obtained catalytic systems were active in the aerobic gas-phase ethanol oxidation under the very mild conditions. The low-loaded bimetallic Au-Cu catalysts did exhibit the highest catalytic activity with almost full conversion and 100% selectivity to acetaldehyde in ethanol oxidation. The most noticeable synergetic effect of the Au-Cu interaction in comparison with the monometallic samples having the same Au or Cu loadings was observed for the systems with the Au:Cu atomic ratio of 1:3. Thus, the 0.2% Au/0.2% Cu/SiO₂ sample produced about 120 g of AA per 1 g of supported gold per hour with full conversion and 100% selectivity at the temperature of 250 °C and under atmospheric pressure. Furthermore, the Au-Cu bimetallic catalysts were very stable under the reaction conditions in several consecutive runs. The highest stability was shown by 0.8% Au/0.8% Cu/SiO₂.

Elucidation of the catalysts structure by different physico-chemical methods revealed that the high activity of the low-loaded Au–Cu catalysts was due to small Au-NPs size and synergistic effect of the strong $\text{Au}^0\text{-Cu}^{2+}$ interaction achieved by applying the redox method for the catalyst preparation, where the Cu^{2+} species were isolated ions but not the copper oxide phase. Strong interaction of isolated Cu^{2+} ions with the support and Au-NPs caused unexpected reduction behavior of the low-loaded Au–Cu catalysts.

The developed catalysts are the prominent systems to apply them in the aerobic gas-phase bioethanol oxidation to acetaldehyde, which is the scope of our further work.

Acknowledgements

Authors thank the Laboratory of structural analysis (ZIOCh RAS) for the STEM study of the catalysts. Authors also thank HASYLAB (DESY, Germany) for the possibility to perform XAS studies, project I-20110468 EC.

References

- [1] T. Takei, N. Iguchi, M. Haruta, *New J. Chem.* 35 (2011) 2227–2233.
- [2] M. Besson, P. Gallezot, *Catal. Today* 57 (2000) 127–141.
- [3] F. Zaccheria, N. Ravasio, R. Psaro, A. Fusi, *Chem. Eur. J.* 12 (2006) 6426–6431.
- [4] E. Santacesaria, A. Sorrentino, R. Tesser, M. Di Serio, A. Ruggiero, *J. Mol. Catal. A: Chem.* 204–205 (2003) 617–627.
- [5] Y. Guan, Y. Li, R.A. van Santen, E.J.M. Hensen, C. Li, *Catal. Lett.* 9 (117) (2007) 18–24.
- [6] J. Trawczyński, B. Bielak, W. Mista, *Appl. Catal. B: Environ.* 55 (2005) 277–285.
- [7] R. Weinstein, A. Ferens, R. Orange, P. Lemaire, *Carbon* 49 (2011) 701–707.
- [8] G. Brett, Q. He, C. Hammond, P. Miedziak, N. Dimitratos, M. Sankar, A.A. Herzog, M. Conte, J.A. Lopez-Sánchez, C.J. Kiely, D.W. Knight, S.H. Taylor, G.J. Hutchings, *Angew. Chem. Int.* 50 (2011) 10136–10139.
- [9] Y. Shen, S. Zhang, H. Li, Y. Ren, H. Liu, *Chem. Eur. J.* 16 (2010) 7368–7371.
- [10] V. Choudhary, D. Dumpre, *Catal. Commun.* 13 (2011) 82–86.
- [11] P. Aghaei, R.J. Berger, *Appl. Catal. B: Environ.* 132–133 (2013) 195–203.
- [12] N. Dimitratos, J.A. Lopez-Sánchez, D. Morgan, A. Carley, L. Prati, G. Hutchings, *Catal. Today* 122 (2007) 317–324.
- [13] C. Pinna, E. Falletta, M. Rossi, *J. Catal.* 260 (2008) 384–386.
- [14] S. Biella, M. Rossi, *Chem. Commun.* (2003) 378–379.
- [15] K.-Q. Sun, S.-W. Luo, Na Xu, B-Qj. Xu, *Catal. Lett.* 124 (2008) 238–242, 3–4.
- [16] C.H. Christensen, B. Joergensen, J. Rass-Hansen, K. Egeblad, R. Madsen, S.K. Klitgaard, S.M. Hansen, M.R. Hansen, H.C. Andersen, A. Riisager, *Angew. Chem. Int. Engl.* 45 (28) (2006) 4648–4651.
- [17] P.-Y. Sheng, G. Bowmaker, H. Idriss, *Appl. Catal. A: Gen.* 261 (2004) 171–181.
- [18] W. Fang, Q. Zhang, J. Chen, W. Deng, Y. Wang, *Chem. Commun.* 46 (2010) 1547–1549.
- [19] T. Mitsudome, A. Noujima, T. Mizugaki, K. Jitsukawa, K. Kaneda, *Adv. Synth. Catal.* 351 (2009) 1890–1896.
- [20] S.M. Tembe, G. Patrick, M.S. Scurrell, *Gold Bull.* 42 (4) (2009) 321–327.
- [21] N. Zheng, G.D. Stucky, *JACS* 128 (44) (2006) 14278–14280.
- [22] V.I. Sobolev, K.Y. Koltunov, O.A. Simakova, A.-R. Leino, D.Y. Murzin, *Appl. Catal. A: Gen.* 433–434 (2012) 88–95.
- [23] O.A. Simakova, V.I. Sobolev, K.Y. Koltunov, B. Campo, A.-R. Leino, K. Kordas, D.Y. Murzin, *ChemCatChem* 2 (12) (2010) 1535–1538.
- [24] J. Bauer, G. Veith, L. Allard, Y. Oyola, S.H. Overbury, S. Dai, *ACS Catal.* 2 (2012) 2537–2546.
- [25] J. Barbier, in: G. Ertl, H. Knözinger, J. Weitkamp (Eds.), *Handbook of Heterogeneous Catalysis*, Wiley-VCH Verlag GmbH, Weinheim, Germany, 1997, pp. 257–264.
- [26] O.A. Kirichenko, E.A. Redina, N.A. Davshan, I.V. Mishin, G.I. Kapustin, T.R. Brueva, L.M. Kustov, W. Li, C.H. Kim, *Appl. Catal. B: Environ.* 134–135 (2013) 123–129.
- [27] C.D. Pinna, E. Falletta, M. Rossi, *J. Catal.* 260 (2008) 384–386.
- [28] S.I. Ginzburg, K.A. Kladyshevskaya, *Handbook on Chemical Analysis of Platinum Metals and Gold*, Nauka, Moscow, 1965 (in Russia).
- [29] M. Shimokawabe, N. Takezawa, H. Kobayashi, *Bull. Chem. Soc. Jpn.* 56 (1983) 1337–1340.
- [30] D. An, Q. Zhang, Y. Wang, *Catal. Today* 157 (2010) 143–148.
- [31] S. Yashnik, A. Salnikov, N. Vasenin, V. Anufrienko, Z. Ismagilov, *Catal. Today* 197 (2012) 214–227.
- [32] A. Stiles, *Catalyst Support and Supported Catalysts*, Chimia, Moscow, 1991, pp. 181–192 (in Russia).
- [33] J. Llorca, M. Dominguez, C. Ledesma, R.J. Chimentro, F. Medina, J. Sueiras, I. Angurell, M. Seco, O. Rossell, *J. Catal.* 258 (2008) 187–198.
- [34] M. Arai, M. Fukushima, Y. Nishiyama, *Appl. Surf. Sci.* 99 (1996) 145–150.
- [35] L.C.A. van den Oetelaar, A. Partrige, S.L.G. Toussaint, C.F.J. Flipse, H.H. Brongersma, *J. Phys. Chem. B* 102 (1998) 9541–9549.
- [36] J. Gong, B.B. Mullins, *J. Am. Chem. Soc.* 130 (2008) 16458–16459.
- [37] M. Boronat, A. Corma, F. Illas, J. Radilla, T. Rodenas, M.J. Sabater, *J. Catal.* 278 (2011) 50–58.
- [38] E. Guan, J.M. Hensen, *Appl. Catal. A: Gen.* 361 (2009) 49–56.
- [39] Y. Guan, E.J.M. Hensen, *J. Catal.* 305 (2013) 135–145.